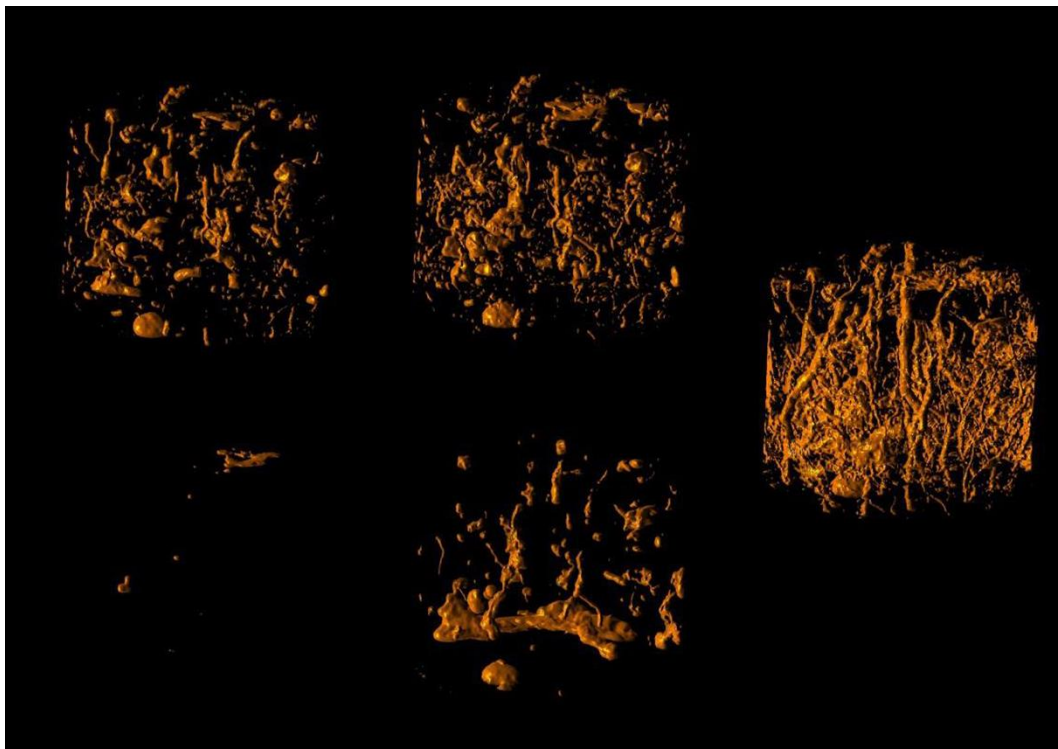Sveriges lantbruksuniversitet
Swedish University of Agricultural Sciences

Department of Soil and Environment

What is the impact of entrapped air on the measurement of saturated hydraulic conductivity of soil?

Maryia Babko

Master's Thesis in Environmental Science

What is the impact of entrapped air on the measurement of saturated hydraulic conductivity of soil?

Maryia Babko

Abstract

X-ray computed tomography was applied to investigate the influence of entrapped air on standard laboratory measurements of saturated hydraulic conductivity K_s in five soil samples. The investigation consisted of five X-ray scans for each sample. Soil samples were saturated by the standard laboratory method from the bottom at the first step. To attain full saturation and explore the difference of entrapped air content on the standard laboratory measurements, a vacuum chamber was used to remove the entrapped air from the initially unsaturated soils and then the samples were again saturated from the bottom. To measure K_s, a measurement device that is based on a constant-head principle was applied. The results showed that the volume of entrapped air greatly depends on how the soil was saturated. Furthermore, the saturated hydraulic conductivity and the entrapped air content were negatively correlated with a strong Pearson correlation coefficient ($r_b = -0.6$). Thus, not considering the existence of entrapped air leads to errors in estimating K_s values.

Popular science summary

Water flow can be defined as one of the most important processes in soil and has been studying for a long time. The water flow in soil is an essential component for hydrological, agricultural and ecological model simulations. The ability of soil to conduct water is characterized by the hydraulic conductivity (K). Hence, the determination of K is vital and it is required as an input parameter in modelling.

Water flow can occur within the soil due to existence of pores. Pore characteristics such as number, size, connectivity and their spatial distribution, direction and orientation affect water flow. There are several studies which have shown that air bubbles can become entrapped in the pores and can stop water flow by blocking water flow paths. The process of entrapped air bubble formation is difficult and not fully understood yet. However, there are some researchers who were trying to look at the entrapped air redistribution by using non-invasive methods that offer the possibility to look inside solid material. This study has used X-ray computed tomography to look at the amount of entrapped air in water saturated soil and to determine the influence of entrapped air on water flow.

The study results have shown that the quantity of entrapped air in the soil depends on the way the soil is saturated. Two types of soil saturation were tested: the standard laboratory method and vacuum soil saturation. The results have shown that the vacuum soil saturation almost completely prevents the entrapped air formation in the soil. The research has also shown that the amount of entrapped air in the soil influence the water flow soil characteristic (K). If the air amount increased the K value decreased. The consideration of entrapped air gives the better estimation of K value. Therefore, this study will contribute to better understanding the water flow in the soil.

Content

1. Introduction

1.1. Hydraulic conductivity

Water flow is one of the most important processes in soil. Water flow influences a lot of other soil processes. It is included in estimations and forecasting of water uptake by plants, evaporation, irrigation requirements and solute transport. It is therefore important for decision-making when managing urban and agricultural resources. The hydraulic conductivity (K) is an important soil characteristic that defines water flow in soil, i.e. the ability of the soil to transport water. Hence, knowledge of soil hydraulic conductivity is essential for the efficient management of soil and water resources for crop production and environmental protection.

To describe water flow in the soil and vadose zone, L.A. Richards combined Darcy's equation that describes saturated water flow with the law of conversation of mass. To calculate water flow with the Richards equation, soil hydraulic properties are required. The soil water retention curve (SWRC) and unsaturated hydraulic conductivity (K_{un}) are required as input characteristics for water flow simulation in the vadose zone. To measure unsaturated hydraulic conductivity directly is often difficult, expensive and time consuming. Thus, there are several methods (models) to estimate unsaturated hydraulic conductivity by using more easily measured soil characteristics, e.g. the saturated hydraulic conductivity (K_s). Therefore, K_s can be used as an input parameter instead of the unsaturated hydraulic conductivity.

There are many methods for K_s estimation either in situ or in the laboratory. When choosing a method, one should consider several factors for a particular situation, including the type of soil, available time, money and equipment and the purpose of the measurement. It is preferable to use the situ measurement due to the fact that this method represents the natural characteristics of the soil (Klute, Campbell, & Soil Science Society of America, 1994). Field measurements are time consuming and require expensive equipment, whilst the laboratory methods are faster and less expensive. Therefore, standard laboratory methods are more frequently used. However, to obtain consistent results from laboratory methods, the soil samples have to be taken carefully and should be representative of the soil structure (Klute et al., 1994).

There are several methods that are well established for determining saturated hydraulic conductivity in the field. They are distinguished by area of implementation 1) methods that applied to areas with shallow water tables, 2) with deep water tables (Klute et al., 1994). The auger-hole method and the piezometer are most commonly used for soils with shallow water tables. Both methods are based on the preparation of a cavity below the water table with the minimum disturbance of the soil. However, there is no simple equation to measure hydraulic conductivity, due to the fact that the water movement in hole is three dimensional (Klute et al., 1994). The double-tub, shallow well pump-in, cylindrical permeameter and air entry permeameter methods are most commonly used for soils with the deep water tables (Klute et al., 1994). All of these methods are time consuming and complicated due to the fact that it is required to measure the saturated hydraulic conductivity above the water table (Klute et al., 1994).

There are two well established and often used laboratory methods to measure saturated hydraulic conductivity: the constant head method and the falling head method, which are based on the measurement of one-dimensional water flow in small cores (Klute et al., 1994). The main difference between these methods is the hydraulic head condition. The constant head method implies steady-

state conditions of pressure head that create steady flow through the sample, which makes it possible to directly apply Darcy's law for K_s estimation. For the falling head method, the head gradient decreases in time so the water flow rate through the sample also decreases through time, which adds some complexity to K_s estimation because differential equations have to be applied in order to calculate K_s (Klute et al., 1994).

1.2. Entrapped air

Entrapped air can be characterized as small isolated bubbles that are not connected to the atmosphere that block water flow paths within the soil, which affects K_s correspondingly. The entrapped air formation and re-distribution in the soil is a complicated process. Its formation is a result of the chaotic nature of water distribution in the soil. Such factors as temperature, pressure and organic carbon concentration influence the content of entrapped air in the soil, but this is still not completely understood (Bormann & Klaassen, 2008; Fodor, Sándor, Orfanus, Lichner, & Rajkai, 2011). Faybishenko (1995) conducted laboratory experiments that showed that entrapped air may be divided into two types: 1) *mobile* that can be moved with the water flow in the soil and easily released from the soil, 2) *immobile* that remains in the pores and can be only dissolved. The content of trapped air depends on how the soil is saturated. In the laboratory experiments reported by Faybishenko (1995), the volume of entrapped air varied from 0.1 to about 10% of the entire soil volume for a loam soil depending on the type of soil saturation, i.e. 1) downward 2) upward 3) primary vacuum extraction or CO_2 injection (Figure1).
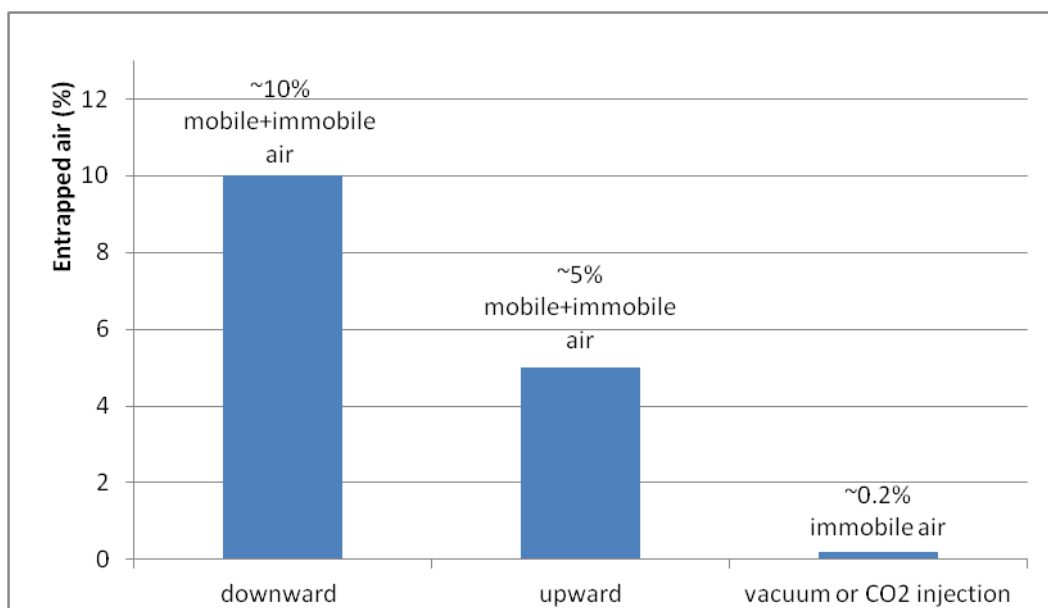
Figure1. Bar Graph of volume of entrapped air in loam soil (Faybishenko, 1995)

The results showed that the volumetric entrapped air content was 10% with downward initial saturation and consisted of both mobile and immobile air. With downward initial saturation, the mobile air leaves the core through the bottom surface during the saturation process. Downward saturation simulates ponded infiltration which may occur in the field. With upward saturation, the entrapped air was around 5% and the mobile air was almost absent. Upward initial saturation duplicates the field processes that occur with a rise of the groundwater level. The mobile air escapes through the top of the core. The difference in mobile air content for the two methods described above can be explained with regard to the ability of air bubbles to move by buoyancy (Archimedes's

principle). Saturation from the base of the core supports the physical process of air buoyancy, while downward initial saturation creates downward forces that offer resistance to the buoyancy forces. Therefore with downward initial saturation more immobile air remains in the soil than with upward saturation. Using vacuum or CO_2 injection, only the immobile air remained with a content of around 0.2 % - almost full saturation was achieved (Faybishenko, 1995).

Near-full saturation with vacuum extraction is achieved basically in two steps: 1) soil samples should be installed in a vacuum chamber with a controlled vacuum, 2) soil samples are subjected to saturation from the bottom with degassed water (Faybishenko, 1995). A second method involves the injection of CO_2 into the soil pore-network in order to replace the pore air. The soil is then saturated with degassed water (Faybishenko, 1995). Because carbon dioxide solubility in water is around 38 times higher than air solubility in water, the amount of entrapped air will be low.

Entrapped air is known to affect the K_s value. There are several studies that investigated the decrease of K_s due to the entrapped air content within the soil (Peck, 1968; Poulovassilis, 1970; Christiansen, 1944; Sakaguchi et.al., 2005). Though the entrapped air distribution is not yet completely understood and not considered when measuring K_s, it is already obvious that the entrapped air has influence on the K_s value (Snehota et.,al., 2015). X-ray computer tomography (CT) is a non-destructive techniques that can be used to investigate the air bubble distribution in soil columns (D. Wildenschild, Vaz, Rivers, Rikard, & Christensen, 2002a).

1.3. X-ray computed tomography

Initially, X-ray computer tomography (CT) was developed for applications in medicine. Later, its use was extended to different scientific disciplines due to the high spatial resolution that the method offers. In recent years, the application of X-ray computed tomography in soil science has increased significantly due to its ability to produce non-destructive images of opaque soil pore structure with good geometrical representation. CT is increasingly used to analyse the pore space networks in the soil due to its ability to visualize 3-D opaque media with the high resolution that improves understanding of the soil pore space structure (D. Wildenschild, Vaz, Rivers, Rikard, & Christensen, 2002b). The non-destructive visualization of the pore space networks can be done to observe the changes in processes of water or air movement with time (Luo, Lin, & Li, 2010). These processes of water and air movements in the soil are crucial for estimation of hydraulic properties, e.g. the saturated hydraulic conductivity (K_s). Hence, the implementation of CT in soil science is increasing. Moreover, CT has been used to define such characteristics and processes as: tortuosity, critical pore diameter, bulk volume, solute transport and to characterize the soil pore network and water content changes with time. Nowadays X-ray CT is reliable and commonly used for a broad range of purposes in soil science (Helliwell et al., 2013; Koestel & Larsbo, 2014; M. Larsbo, Koestel, & Jarvis, 2014; Mats Larsbo, Koestel, & Jarvis, 2014; Paradelo et al., 2016; Dorthe Wildenschild & Sheppard, 2013).

There are several studies (Dohnal, Jelinkova, Snehota, Dusek, & Brezina, 2013; Jelinkova, Snehota, Pohlmeier, van Dusschoten, & Cislerova, 2011; Snehota et al., 2015) that were conducted with the aim to analyse the entrapped air distribution in the soil. However, the entrapped air redistribution still it is not yet entirely understood and not considered when measuring K_s, it is already obvious that the entrapped air has influence on the K_s value, which is why the X-ray CT can be an efficient tool to look at the entrapped air distribution.

Therefore, the aim of this study is to use X-ray CT to define and compare entrapped air content for vacuum and standard laboratory methods of initial soil saturation and to determine the entrapped air effect on the saturated hydraulic conductivity.

I am distinguishing two objectives of this study: 1) to visualize entrapped air content by using X-ray CT, 2) to quantify the influence of entrapped air on the hydraulic conductivity K_s by using a constant-head laboratory method

.

2. Materials and Methods

2.1. Soil sampling

Five undisturbed soil samples were taken in Ås, about 30 km from Oslo, in south-east Norway. The soil is classified as a Stagnosol, and it is primarily composed of reduced clays and silts. The samples were taken from different depths, from 5 cm up to 55 cm below the soil surface, using aluminum columns with an inner diameter of 6.5 cm, and a cross-sectional area of 33.2 cm^2. The samples were trimmed at the top and the bottom surfaces to the same length as the aluminum cylinders, resulting in a bulk soil volume of 199.1 cm^3.

2.2. X-ray scanner

A GE Phoenix v|tome|x X-ray scanner was used (GE, 2014) to collect 3-D X-ray images. The samples were scanned at a resolution of 40 μm. The cathode voltage was adjusted to 150 kV and electron transition was adjusted to 280 mA for all scanned samples. Two thousand radiographs were obtained for each soil sample. These radiographs were reconstructed using the software package GE datos|x (GE, 2014) which uses the Feldkamp algorithm (Feldkamp, Davis, & Kress, 1984) to obtain a 3D image. The radiograph reconstructions were carried out using the datos|x in-built median filter and beam-hardening correction approach.

2.3. Measurement device for the saturated hydraulic conductivity

The constant-head method was used to measure the saturated hydraulic conductivity of the cores in the laboratory (Figure 2).

Figure 2. Photo of the measurement device for the saturated hydraulic conductivity

The method is based on an application of Darcy's law (Klute et al., 1994). The saturated hydraulic conductivity K_s was calculated by using eq.1:

$$K = \frac{V\,L}{A\,t\,(H_2 - H_1)} \tag{1}$$

where V is the water volume that goes through the soil column (ml), A is the cross sectional area of the soil sample (cm^2), t is the time for collecting the water volume (s), L is the soil column length (cm) and H_2-H_1 is the head difference across the soil sample (i.e. between the funnel water head level and the soil sample water level)(cm).

To use the K_s measurement device, installation of extra equipment (the plastic forms (cups), base, bolt and rubber band) at the top part of the soil column is required. These installations take around 2 minutes per sample. Moreover, the soil samples are taken out of water to install extra equipment (Figure 3).
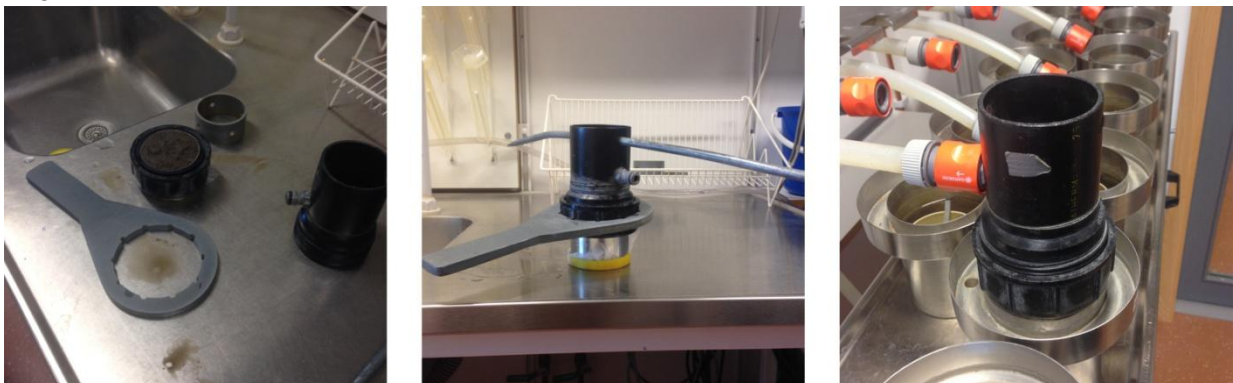

Figure 3. Photos of the installation of extra equipment on constant-head device for K_s measurement

To saturate the soil cores with minimum amount of free and entrapped air the vacuum chamber was constructed (Figure 4).
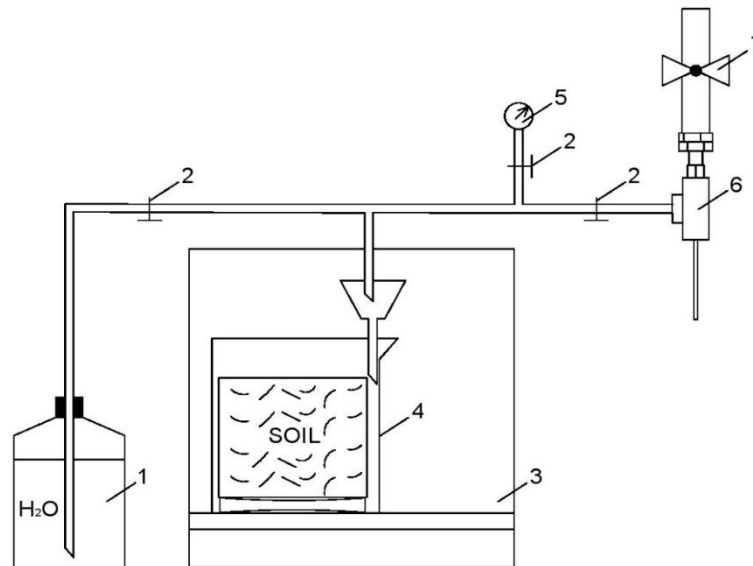

Figure 4. Principal scheme of the vacuum soil saturation where 1, cooled-down boiled water reservoir; 2, clamps; 3, desiccator; 4, plastic beaker; 5, vacuometer; 6, aspirator; 7, water tap.

The soil columns were put in a chamber as shown in Figure 4. The aspirator (6) was installed to create a near-vacuum using the Venturi effect. A pressure difference of approximately 100 kPa between the room atmosphere and inside the desiccator was measured and controlled by the pressure gauge (5). Once the samples were placed in the chamber, the tap was open; the aspirator with the adjustable venture valve used the running water in order to evacuate the desiccator, and the soil samples that were inside it. When the required level of vacuum was achieved, the clamp (near the aspirator) was closed and the other clamp (near the water reservoir) was opened in order to saturate the soil samples. Saturation was carried out by upward water flow that created a possibility for the entrapped air that may still be in the core, to leave the soil through the upper surface. Vacuum saturation was carried out slowly to make sure that all air was removed. These two stages of vacuuming and adding water were repeated five times until full soil saturation. It took a day to complete the saturation process.

2.5. Experimental procedure

As a first step, the soil samples were weighed. Then they were placed on a sand bed to equilibrate to a reference matric potential of -100 cm for thirteen days. The bottom surface of each column was covered by a nylon cloth which was fixed with a rubber band. Next, the soil columns were scanned with the aim to get an image of the X-ray resolvable macropore networks in the soil sample, which were expected to be air-filled at the established matric potential and therefore easily distinguishable from the rest of the soil volume.

The samples were then weighed again and placed in a box to slowly saturate them from the bottom. To prevent additional air bubbles in the soil, degassed water was used. The state of degassed water was achieved through boiling and then cooling to room temperature in an air-tight bottle. This degassed water was used for the saturation. The soil saturation process lasted for twelve days, adding 5 mm of degassed water each day during the saturation process until full saturation of the sample was achieved. Then, each soil sample was put in a plastic beaker with degassed water inside for another

round of X-ray imaging. This second scan was performed in order to capture the resolvable entrapped air bubbles after the standard laboratory method of saturation.

The next step was to measure the hydraulic conductivity, K, of the soil cores using the above describe measurement device. The constant head measurement device is placed in temperature controlled room, so that the temperature of the water and air was constant during the measurements (+19.5 ºC). The measurement of K_s was performed three times and the mean value was taken for later analyses. Before the K_s measurement, the device requires the placement of plastic forms (cups), base, bolt and rubber band in the top part of the soil column. All these installations require the soil sample to be taken out of the water. After the plastic forms (cups), base, bolt and rubber band were installed, the soil column was placed in the measurement device. The installation was done sequentially. The water was not delivered to the samples until all samples with their plastic forms on top are placed in the measurement device. It took around 10 minutes to place them all. Hence, the installation of the extra equipment and the time that the samples are out of the water may lead to a significant drainage of water and air penetration into the soil column.

The process of soil samples installation on measurement device is shown Figure 5.
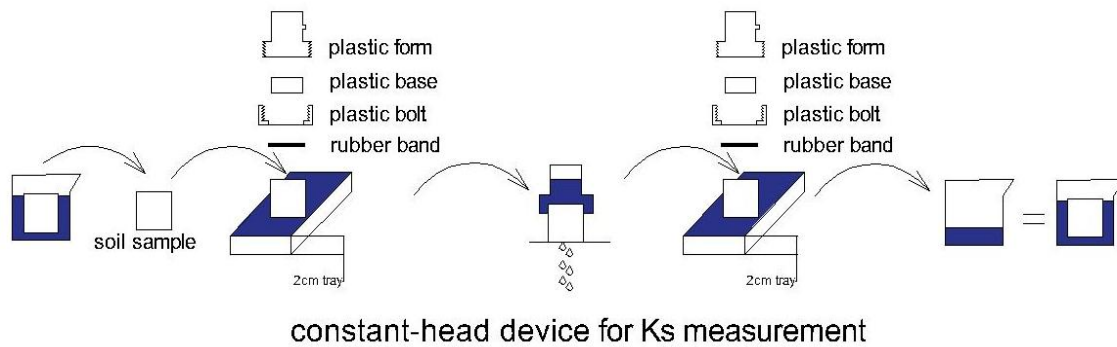
Figure 5. Sketch of the soil sample installation in constant-head device for K_s measurement

After the hydraulic conductivity measurement, all the extra parts were uninstalled, which took around 2 minutes, and then each soil column was placed in the beaker again. After that, the soil samples were scanned again in order to check if there were some changes in the soil porous structure. After the third round of X-ray scans was completed, the soil columns were placed on the sand bed for fourteen days, once again to equilibrate to the reference matric potential of -100 cm to re-establish similar soil water contents as in the beginning of the experiment.

The samples were then slowly saturated under near-vacuum as explained above. The fourth X-ray scan was done after the vacuum saturation was completed to obtain the water filled pore structure and the distribution of residual air-bubbles. Further, the samples were weighed then the saturated hydraulic conductivities were measured using the constant-head method as described above. To see if the constant head measurement process influenced the water filled macropore-network, a fifth scan was carried out.

The described above stages of the experiment are graphically demonstrated below (Figure 6).

Figure 6. Sketch of the experiment

2.6. Image analyses

2.6.1. Image processing

The Fiji software package (Schindelin et al., 2012) which is based on ImageJ (Schneider, Rasband, & Eliceiri, 2012) was used for image analysis. As a first step, all images were scaled to reduce the image processing time by a factor 4 and further analysis was done at a resolution of 160 µm. The SoilJ plugin (Koestel, 2016) was used to automatically move the columns to an upright position in the center of the image canvas and to detect the column outlines.
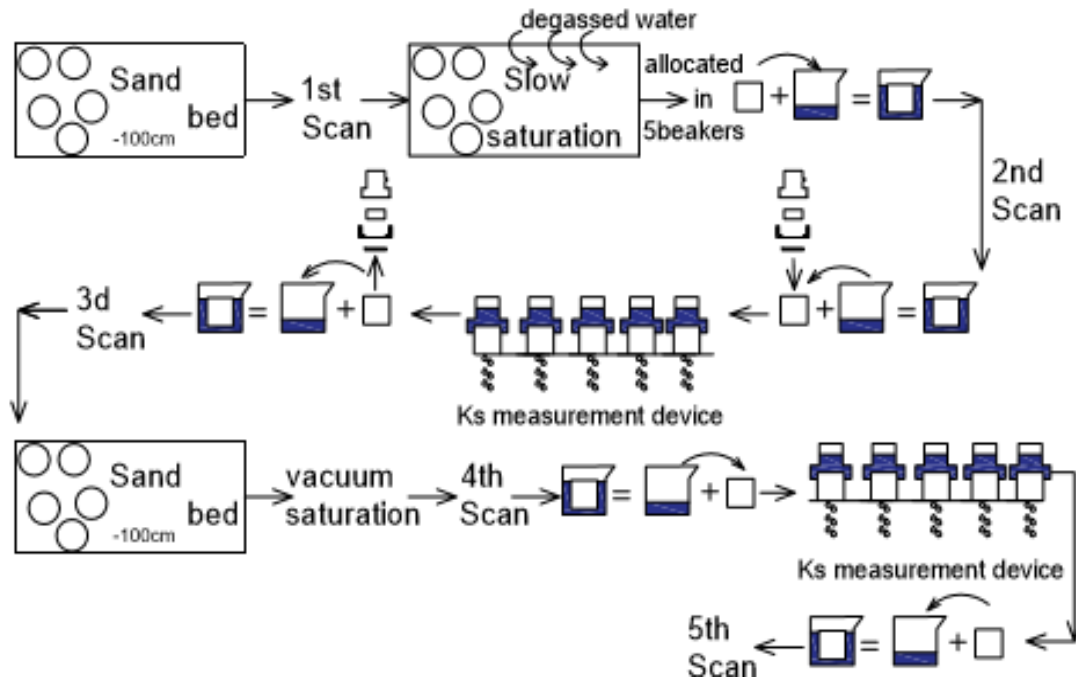
2.6.2. Normalization

The SoilJ plugin was used to normalize the gray-values in the images, i.e. the gray-values of air, water and walls were adjusted so that they all exhibited approximately identical values in all investigated X-ray images. The 3-D image from the second, third, fourth and fifth rounds of scans were submerged in the water during the scanning and all these 3-D images contain 4 major phases: air, water, soil matrix and wall. The 3-D image from first scan only had 3 phases: air, soil matrix and wall. Due to this fact, the normalization process was done in two steps. As a first step, the 3-D image from the second, third, fourth and fifth rounds of scans were normalized to water and wall values of approximately 10.000 and 20.000 correspondently. The Histogram tool was then applied to find the grey value of air. The values of the air phase ranged around 5000. Hence, for the second step the 3-D image from first scan were normalized for gray values of 5.000 and 20 000 for air and column walls respectively.

2.6.3. Registration

The Registration plugin (Preibisch, Saalfeld, Schindelin, & Tomancak, 2010) was used to match the common points of different 3-D images. Each slice was used as a reference point for the next slice to align with. The descriptor-based registration (2d/3d) plugin can process only with two images simultaneously, which increased the time needed for image analyses. The 3-D image of the

unsaturated soil was used as a reference for the respective images from the other 4 scanning rounds and used as a reference 3-D image for later subtraction.

2.6.4. Segmentation

The intensity segmentation of the 3-D image was done by using a constant threshold for all images. A gray-value of 8000 was determined as a threshold upon visual inspection. All values below 8000 were assigned to air, and values above 8000 were assigned to soil matrix. By applying the threshold gray value of 8000 to the 3-D images that were used as reference images (unsaturated soil columns), binary images of the macropore space were created. The same threshold was applied for the remaining 3-D images to obtain binary images of the entrapped air. All images were checked for segmentation artifacts with particular attention paid to the top and bottom of the column. The first and last slices were excluded to create equal soil column depths for all images.

2.6.5. Subtraction

Binary images of the water-filled pores were obtained by using the ImageJ "Image calculator" (Schneider et al., 2012). The 3-D images of unsaturated soil were used as a reference for the other images (1.after laboratory saturation, 2.laboratory saturation and K_s measurement, 3. after vacuum saturation, 4. vacuum saturation and K_s measurement). The binary images with entrapped air were subtracted from the binary images of the pore space structure to obtain the binary images of water-filled pores.
Three types of binary images were eventually created, depicting the macropore space, the entrapped air and the water-filled macropore space, respectively.

2.6.6. Pore space analysis

The pore space analysis function from the SoilJ plugin (Koestel, 2016) was applied to calculate the soil properties on the binary images such as macropore volume, fractal dimension and percolating pore volume. The macroporosity was calculated from binary images as the ratio of volume (voxels) that was defined as pores to the entire soil volume (voxels). Macropore volume was calculated for each slice in the vertical direction through the core. Fractal dimension was estimated to see the heterogeneity of macropore volume distribution. The BoneJ plugin (Doube et al., 2010) was used to obtain pore thickness. Thickness is interpreted as a largest diameter of the sphere that fits into the macropore (Mats Larsbo et al., 2014). The GeoDict software ("GeoDict," n.d. Kaiserslauten) was used to determine critical pore diameters and path length. The path length is determined as a continuous way from top to bottom within the soil sample. Critical pore diameter is the smallest diameter along the path that connects the top to the bottom. It is given by the size of the largest sphere that can pass though the sample.

3. Results and Discussion

3.1. Morphological features of the macropore networks

The vertical macroporosity distribution calculated for each horizontal slice from SoilJ is shown in Figure 7.
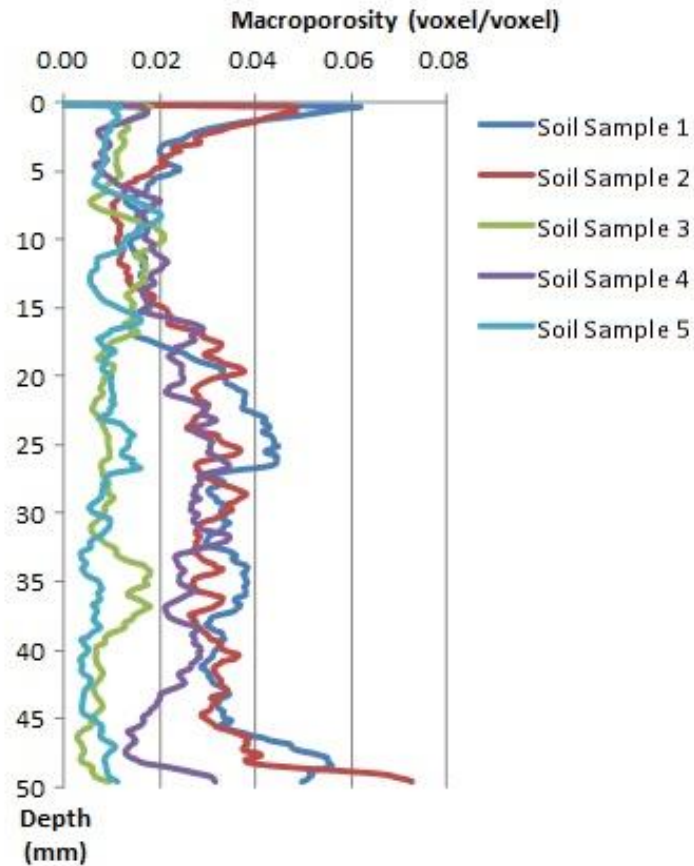
Figure 7. Vertical distribution of macroporosity within the samples

The variation of macroporosity in depth for Soil Samples 1 and 2 is larger than for the other samples. The macroporosity varied from 0.01 to 0.06 for Sample 1 and from 0.01 to 0.07 for Sample 2. The soil samples were taken from different depth (Table 1).

Table 1. Soil sampling at each depth

	Depth (cm)
Soil Sample 1	5-10
Soil Sample 2	20-25
Soil Sample 3	30-35
Soil Sample 4	50-55
Soil Sample 5	50-55

Results of vertical distribution of macroporosity within the samples might suggest that the macroporosity decreased with depth, as also shown by Katuwal et al., (2015) and Luo et al. (2010)

3.2. Entrapped air
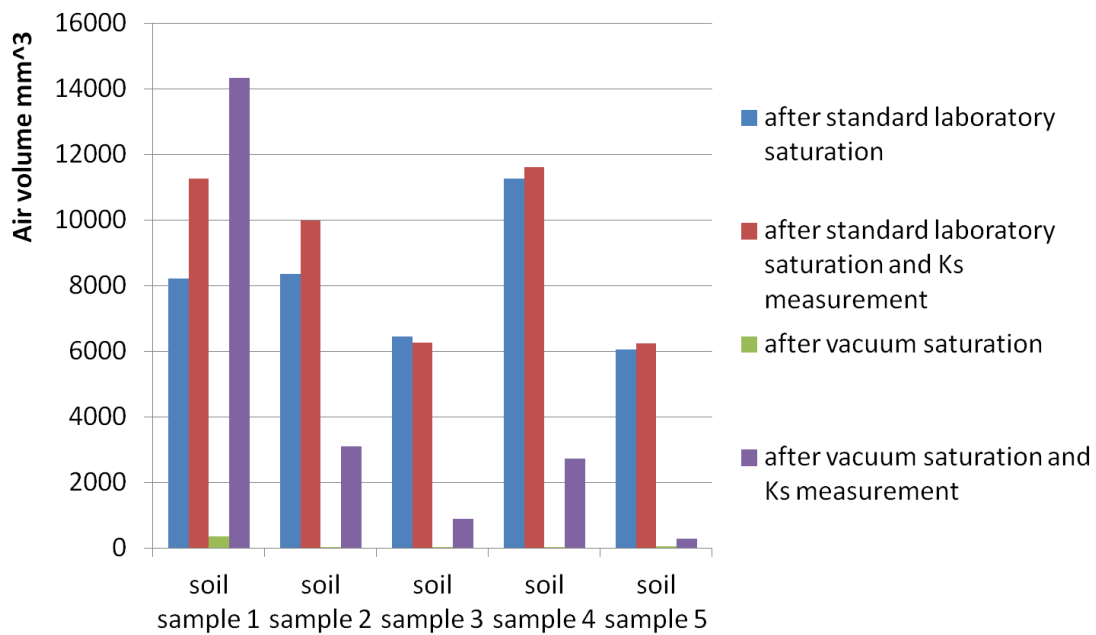
Figure 8. Graphical representation of air volume (mm^3) in five soil samples

Figure 8 illustrates air volumes (mm^3) in the five soil samples after four different stages: 1) after standard laboratory saturation, 2) after standard laboratory saturation and K_s measurement, 3) after vacuum saturation and 4) after vacuum saturation and K_s measurement. Overall, the air volume increased between stages 1-2 and 3-4 (Figure 8). In most samples, the air volume after the laboratory saturation and K_s measurement was higher than after other stages. The smallest air volume was observed after vacuum saturation. These results support the findings of Faybishenko (1995) and Smith & Browning (1946) that soil saturation under a vacuum decreased air content (Table 2).
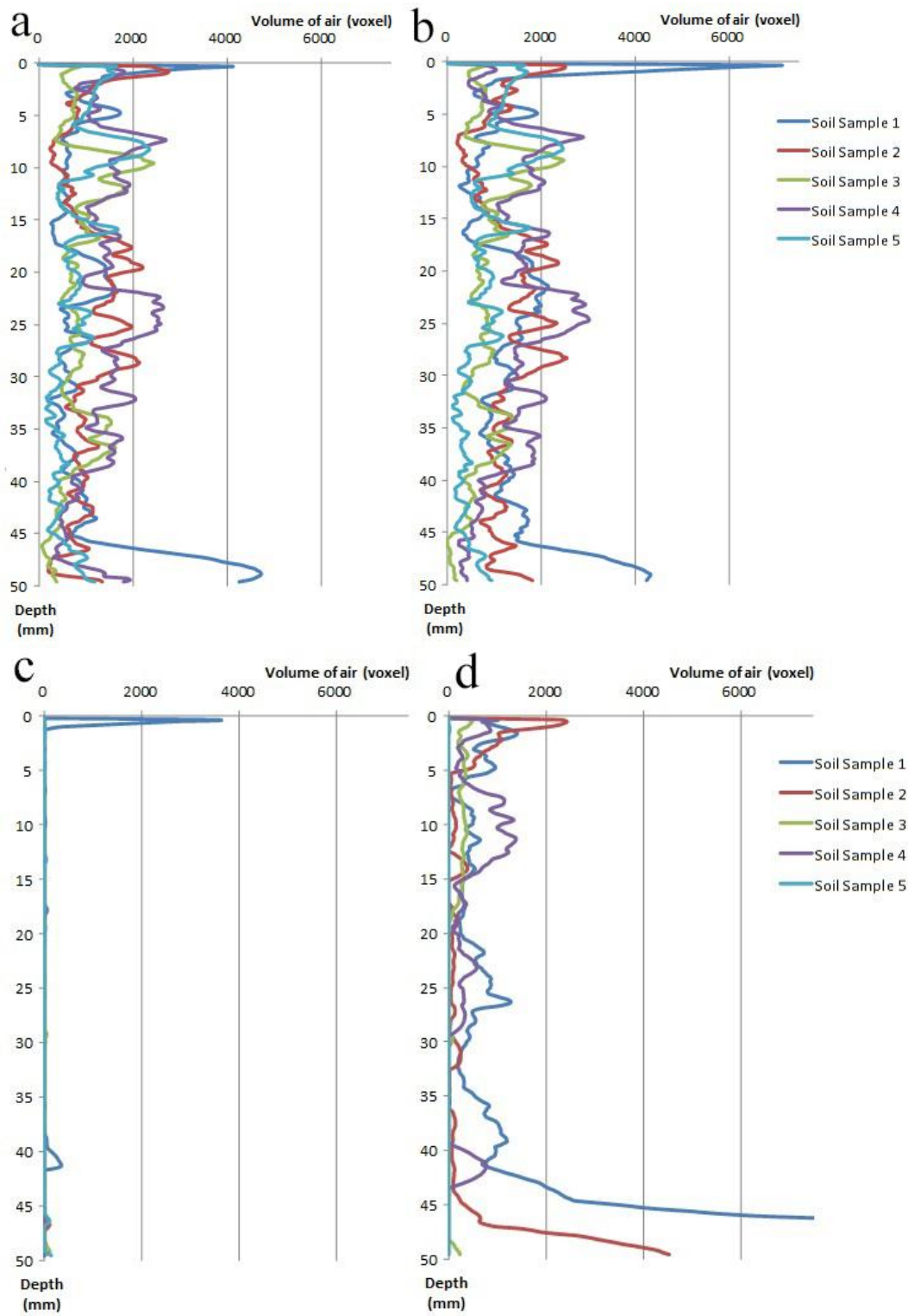
Figure 9. Vertical distribution of the entrapped air volume in five soil samples (a) after laboratory saturation, (b) after laboratory saturation and K_s measurement, (c) after vacuum saturation and (d).after vacuum saturation and K_s measurement

Table 2. Macroporosity and the entrapped air content (% of entire soil column volume)

	Soil Sample 1	Soil Sample 2	Soil Sample 3	Soil Sample 4	Soil Sample 5
macroporosity	3.06	2.83	1.06	2.19	0.89
after standard laboratory saturation	0.78	0.80	0.62	1.07	0.58
after standard laboratory saturation and K_s measurement	1.07	0.95	0.60	1.11	0.60
after vacuum saturation	0.03	0.00	0.00	0.00	0.00
after vacuum saturation and K_s measurement	1.37	0.29	0.09	0.26	0.03

The entrapped air volume with the standard laboratory method of saturation varied from 0.62% to 1.07% of the entire soil volume. Meanwhile, the volume of entrapped air under the vacuum saturation was hardly measurable(0-0.03%) (Table 2). If the entrapped air is found as the proportion of volume of entrapped air to the macropore volume, it varies from 25.6% to 64.67% for the standard laboratory method and from only 0.04% till 1.08% for the vacuum method of soil saturation (Table 3).

Table 3. The entrapped air content (% of the macropore volume)

stages	Soil Sample 1	Soil Sample 2	Soil Sample 3	Soil Sample 4	Soil Sample 5
after standard laboratory saturation	25.61	28.13	58.22	49.01	64.67
after standard laboratory saturation and K_s measurement	35.10	33.59	56.39	50.52	66.76
after vacuum saturation	1.08	0.05	0.27	0.04	0.43
after vacuum saturation and K_s measurement	44.71	10.40	8.05	11.83	2.91

The air volume increased between stages 1 and 2 in all samples except for the third sample (Figure 8). The most likely explanation for this is that when installing the soil columns on the K_s measurement equipment, air penetration into the soil columns was possible as the installation process required the soil columns to be lifted out of the water several times.

In the third sample where the air volume decreased between stages 1 and 2, a large macropore had become saturated after the K_s measurement (see figure 10).

Figure 10. Images of air volume of Soil Sample 3 (a) after laboratory saturation, (b) after laboratory saturation and K_s measurement

The difference in air volume between stages 1 and 2 can be visually identified in Figure 10. The red circle points out the approximate position of the decreased air content in column 3 (Figure 10b). Air bubbles may have blocked the pore path during the standard laboratory saturation (Figure 10a), but either due to dissolution or to exterior factors, the bubble was released from the soil core (Figure 10b). The dissolution of the entrapped air can be explained either by temperature and pressure changes within the soil (Orlob & Radhakrishna, 1958) or by aerobic bacterial processes as soil bacteria produce highly soluble carbon dioxide gas that has a greater solubility in water than air (Christiansen, 1944; Stumm W & Morgan J. J, 1996).

The vertical distribution of the entrapped air volume for stages 1 and 2 (Figure 10) in Soil Sample 3 is shown in Figure 11.
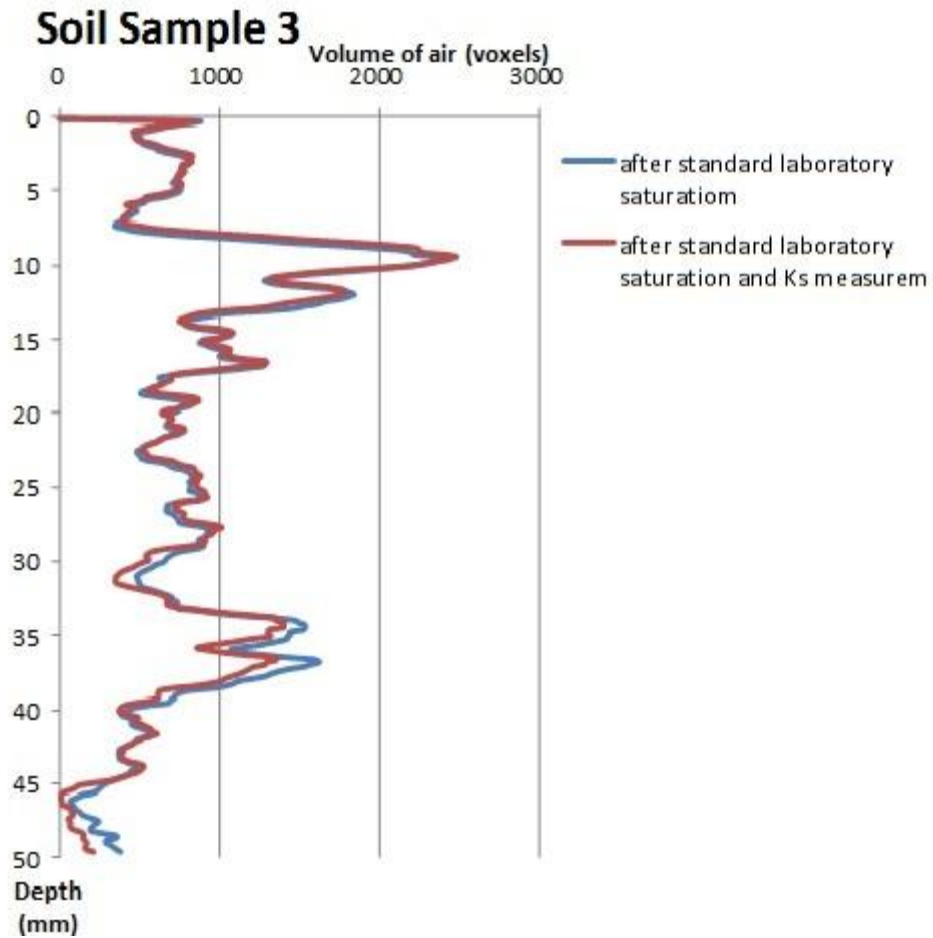
Figure 11. Vertical distribution of entrapped air volume in Soil Sample 3 (blue) after laboratory saturation, (red) after laboratory saturation and K_s measurement

The red line mostly follows the shape of the blue one. Small differences can only be found in a few extreme points in the lower part of the column. This ties up with previous image representations of entrapped air (Figure 10), where it was possible to distinguish more entrapped air bubbles after stage 1 (laboratory saturation).

While the air volume differences between stages 1-2 and 3-4 generally varied among soil samples by only around 1000 mm^3, these differences in Soil Sample 1 were as large as 2000-12000 mm^3 (Figure 8). Therefore, it is interesting to visualize the air volume content for the Soil Sample 1 after all stages of soil saturation (Figure 12).
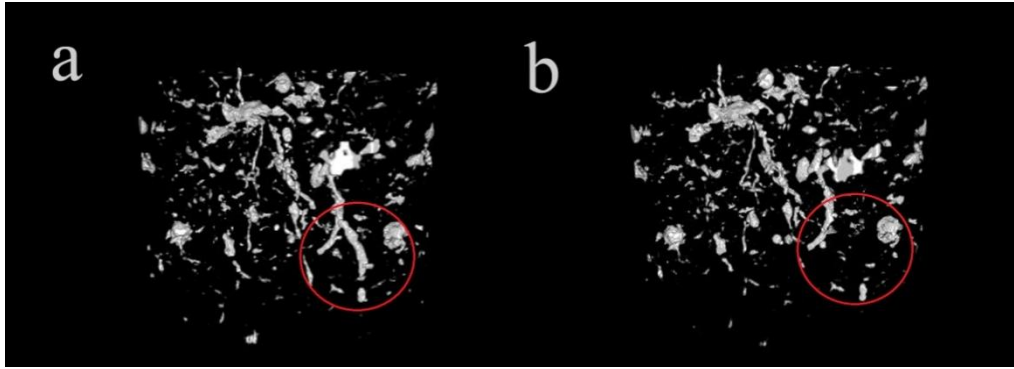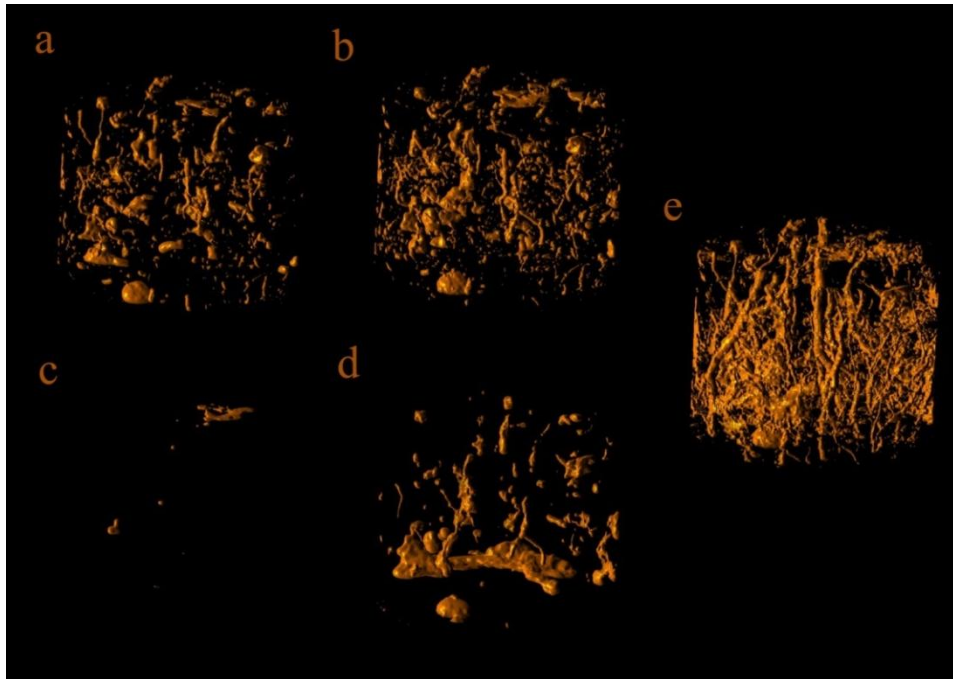
Figure 12. Images of air volume of Soil Sample 1(a) after laboratory saturation, (b) after laboratory saturation and K_s measurement, (c) after vacuum saturation, (d) after vacuum saturation and K_s measurement and (e) image of unsaturated soil. The orange color represents the pore structures which are larger than 0.32 mm.

The vertical distributions of the entrapped air of Soil Sample 1 are shown in Figure 13.
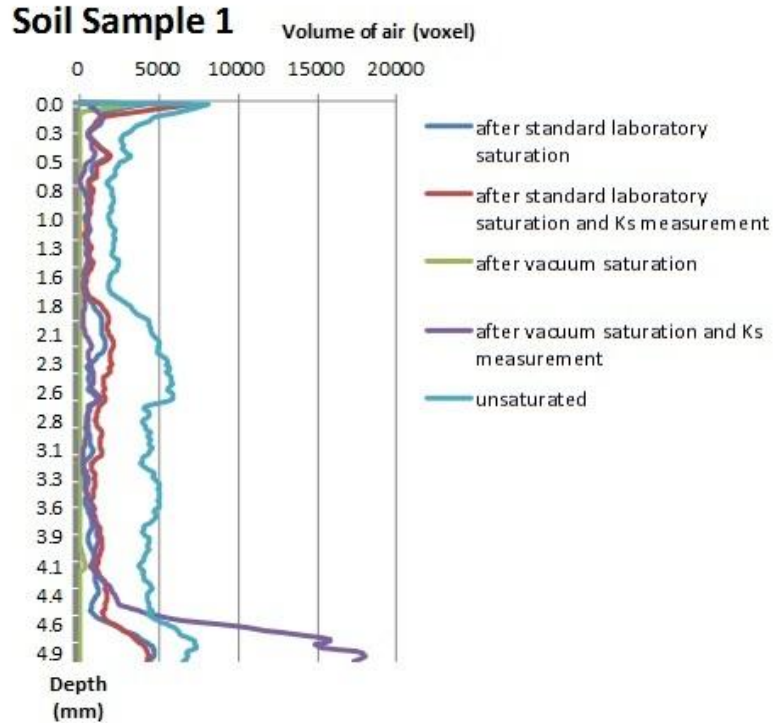
Figure 13. Vertical distribution of entrapped air volume in Soil Sample 1

Overall, the volumes of entrapped air were different for different parts of the columns. At the top and bottom of the core it was higher, whilst it was lower in the middle of the soil core. Moreover, the air

volume after vacuum saturation and K_s is much higher at the bottom of the column than the air volume of the unsaturated soil, which is only possible because a new, large, air gap had appeared. It may have happened during the K_s measurement, by installing the plastic part on the top (Figure 5) and due to the frequent movements of soil column.

3.3. Relationship between entrapped air and K_s

Results for the saturated hydraulic conductivities measured in the laboratory are shown in Table 3.

Table 3. Hydraulic conductivity values

	K s	
	saturation	vacuum saturation
soil sample	cm/h	cm/h
Soil Sample 1	156.7	172.2
Soil Sample 2	213.4	237.3
Soil Sample 3	9.8	7.5
Soil Sample 4	79.2	195.0
Soil Sample 5	0.0	0.70

Overall, the saturated hydraulic conductivity was higher after vacuum saturation than after the standard laboratory method of saturation, except for the third sample, where the saturated hydraulic conductivity decreased. This might be due to the fact that not only entrapped air influences hydraulic conductivity, but also such factors as microbiological activities and chemical processes (Allison, 1947). The second possible reason might be the soil pore structure. Percolation volume of the soil column 3 was calculated from the binary image by recognizing macropores that are connected from top to bottom. The percolation volume was calculated for all binary images and was zero for this core. This raises the question why it was possible to measure hydraulic conductivity on this column if there are no connected pores from top to bottom. The existence of hydraulic conductivity value is explained by taking into account the spatial resolution of the images. The study was conducted with the dimensional resolution of 160 μm so the soil structure less than 0.32 mm was not recognized and not available for analysis. Therefore, some pores that are smaller than 0.32 mm contributed to the water flow within the soil column 3.The same was true for Soil Sample 5. The saturated hydraulic conductivity increased with the vacuum saturation, but no percolating pore volume was found.

The relationship between saturated hydraulic conductivity and entrapped air content is depicted in Figure 14.
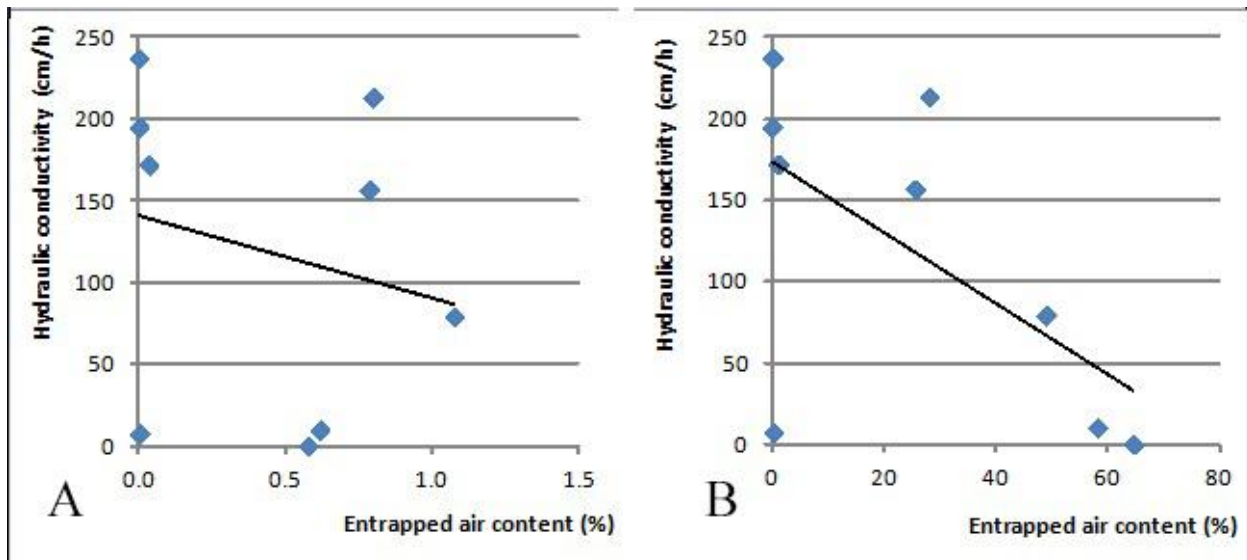
Figure 14. Saturated hydraulic conductivity as a function of entrapped air content (A) relationship with the entrapped air that was found as the proportion of volume of entrapped air to the bulk soil volume, (B) relationship with the entrapped air that was found as the proportion of volume of entrapped air to the volume of the macropore volume

The entrapped air content was negatively correlated with saturated hydraulic conductivity (Figure 14), supporting the findings of previous studies (Faybishenko, 1995; Sakaguchi, Nishimura, & Kato, 2005; Snehota et al., 2015) that noted the significance of volume of entrapped air in the core and its influence on the decrease of hydraulic conductivity value. Pearson correlation coefficients were measured to assess the relationships between the saturated hydraulic conductivity and the entrapped air content (r_a =-0.2, r_b =-0.6). A stronger negative linear relationship was found for the relationship between the saturated hydraulic conductivity and the entrapped air as the proportion of the volume of entrapped air to the volume of the macropore volume than for the relationship with the entrapped air as the proportion of volume of entrapped air to the volume of the bulk volume (r_b =-0.6, Figure 14). The morphologic characteristics of the macropore network and the water-filled macropore-space for stages 2 – 5 are shown in Table 4.

Table 4. Pore network morphology measures and state variables: Macro, total macropore volume (voxels); D, fractal dimension; Per, macropores percolation volume(voxels); Th mean, mean thickness of macropores; $d_{critical}$, critical pore diameter(mm); Path, macropores path length(mm); K_s, saturated hydraulic conductivities (cm/h).

The morphologic characteristics of the macropore network of unsaturated soil samples

	Macro	D	Per	Th mean	d critical	Path	K_s
Soil Sample 1	1253068	2.10	570411	8.62	0.96	57.83	156.72
Soil Sample 2	1160139	2.27	352185	6.28	0.96	52.69	213.38
Soil Sample 3	433150	1.75	0	7.82	0.00	0.00	9.83
Soil Sample 4	897191	1.99	153166	10.07	0.32	61.21	79.17
Soil Sample 5	365041	1.79	0	7.35	0.00	0.00	0.00

The morphologic characteristics of the macropore network of soil samples after standard laboratory saturation

	Macro	D	Per	Th mean	d critical	Path	K_s
Soil Sample 1	23761	2.02	226609	6.08	0.96	57.55	156.72
Soil Sample 2	21950	2.23	261070	3.78	0.96	52.69	213.38
Soil Sample 3	5088	1.69	0	4.42	0.00	0.00	9.83
Soil Sample 4	19863	1.92	150805	8.40	0.32	61.26	79.17
Soil Sample 5	4229	1.80	0	2.37	0.00	0.00	0.00

The morphologic characteristics of the macropore network of soil samples after standard laboratory saturation and K_s measurement

	Macro	D	Per	Th mean	d critical	Path	K_s
Soil Sample 1	22856	2.04	309325	5.58	0.96	57.87	156.72
Soil Sample 2	16905	2.14	116462	3.90	1.01	53.55	213.38
Soil Sample 3	5108	1.67	0	4.65	0.00	0.00	9.83
Soil Sample 4	12660	1.93	112062	6.20	0.32	61.63	79.17
Soil Sample 5	3621	1.72	0	2.55	0.00	0.00	0.00

The morphologic characteristics of the macropore network of soil samples after vacuum saturation

	Macro	D	Per	Th mean	d critical	Path	K_s
Soil Sample 1	32432	2.06	501064	7.22	0.96	57.78	172.17
Soil Sample 2	29245	2.21	394736	5.38	0.96	52.65	237.32
Soil Sample 3	10828	1.71	0	6.83	0.00	0.00	7.53
Soil Sample 4	22434	1.94	151837	8.45	0.32	61.22	194.98
Soil Sample 5	9211	1.77	0	5.89	0.00	0.00	0.70

The morphologic characteristics of the macropore network of soil samples after vacuum saturation and K_s measurement

	Macro	D	Per	Th mean	d critical	Path	K_s
Soil Sample 1	25981	2.05	438996	5.90	0.45	64.99	172.17
Soil Sample 2	25008	2.17	293696	4.99	1.01	53.32	237.32
Soil Sample 3	9845	1.70	0	6.64	0.00	0.00	7.53
Soil Sample 4	19863	1.92	150805	8.40	0.32	61.26	194.98
Soil Sample 5	9135	1.77	0	5.96	0.00	0.00	0.70

Pearson correlation coefficients were measured to assess the relationship between hydraulic conductivity and pore network morphology measures (Table 5).

Table 5. Pearson correlation coefficients of pore network morphology measures and K_s where: Macro, total macropore volume; D, fractal dimension; Per, macropores percolation volume; Th mean, mean thickness of macropores; $d_{critical}$, critical pore diameter; Path, macropores path length; K_s, saturated hydraulic conductivities

Correlations of pore network morphology measures and K_s of unsaturated soil samples

	Macro	D	Per	Th mean	d critical	Path	K_s
Macro	1.00						
D	0.92	1.00					
Per	0.94	0.81	1.00				
Th mean	0.09	-0.20	0.03	1.00			
d critical	0.96	0.94	0.95	-0.17	1.00		
Path	0.92	0.83	0.77	0.37	0.80	1.00	
Ks	0.94	**0.99**	0.86	-0.23	**0.97**	0.80	1.00

Correlations of pore network morphology measures and K_s of soil samples after standard laboratory saturation

	Macro	D	Per	Th mean	d critical	Path	K_s
Macro	1.00						
D	0.84	1.00					
Per	0.97	0.94	1.00				
Th mean	0.58	0.10	0.38	1.00			
d critical	0.90	0.91	0.96	0.21	1.00		
Path	0.98	0.77	0.91	0.70	0.80	1.00	
Ks	0.89	0.96	**0.98**	0.20	**0.97**	0.80	1.00

Correlations of pore network morphology measures and K_s of soil samples after standard laboratory saturation and K_s measurement

	Macro	D	Per	Th mean	d critical	Path	K_s
Macro	1.00						
D	0.90	1.00					
Per	0.95	0.74	1.00				
Th mean	0.54	0.33	0.57	1.00			
d critical	0.94	0.96	0.81	0.28	1.00		
Path	0.87	0.89	0.77	0.67	0.79	1.00	
Ks	0.88	**0.98**	0.70	0.27	**0.98**	0.81	1.00

Correlations of pore network morphology measures and K_s of soil samples after vacuum saturation

	Macro	D	Per	Th mean	d critical	Path	K_s
Macro	1.00						
D	0.92	1.00					
Per	0.97	0.89	1.00				
Th mean	0.12	-0.18	-0.05	1.00			
d critical	0.97	0.95	0.99	-0.14	1.00		
Path	0.91	0.83	0.80	0.39	0.80	1.00	
Ks	0.91	**0.93**	0.80	0.16	0.84	**0.96**	1.00

Correlations pore network morphology measures and K_s of soil samples after vacuum saturation and K_s measurement

	Macro	D	Per	Th mean	d critical	Path	K_s
Macro	1.00						
D	0.95	1.00					
Per	0.95	0.87	1.00				
Th mean	-0.20	-0.40	-0.32	1.00			
d critical	0.84	0.96	0.72	-0.46	1.00		
Path	0.95	0.84	0.86	0.11	0.71	1.00	
Ks	**0.94**	0.92	0.79	-0.03	0.88	**0.94**	1.00

The strongest Pearson correlation coefficients between K_s and pore network morphology measures are marked by bold font (Table 5). Overall, the critical pore diameter and the fractal dimension had the strongest Pearson correlation coefficients with K_s (Table 5).

By looking at critical pore diameters values at the different saturation stages it is possible to see that there are only small changes in critical pore diameter after using the K_s measurement device for Soil Sample 2 and the largest change appears after stage 4 (after vacuum saturation and K_s measurement) for Soil Sample 1, where critical pore diameter halved(Table 4). Otherwise, the critical pore diameter remained at the value derived from the water-free macropore network. Therefore, if it is assumed that K_s is approximately proportional with the square of the critical pore diameter, no correlations between the amount of entrapped air and saturated hydraulic conductivity should be expected. My study has shown a correlation between entrapped air and K_s with quite a strong Pearson correlation coefficient (r_b =-0.6, Figure 14). However, the Ks value increased significantly after vacuum saturation only for Soil Sample 4 (Table 3).

The relationship between saturated hydraulic conductivity and critical pore diameter is depicted in Figure 15.
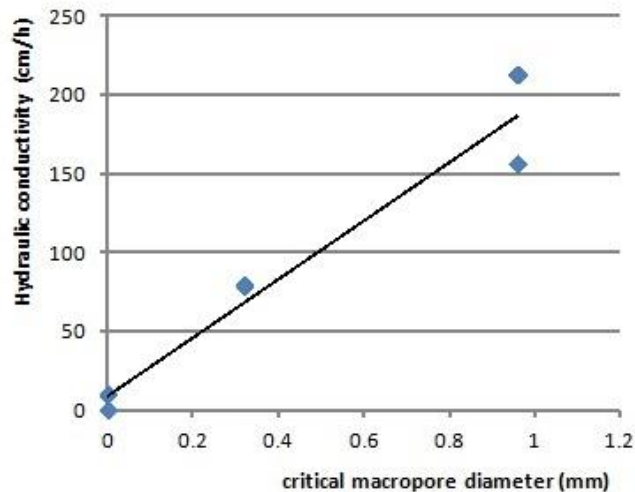

Figure 15. Saturated hydraulic conductivity as a function of critical pore diameter

The critical pore diameter was positively correlated with saturated hydraulic conductivity (Figure 15), Pearson correlation coefficient was measured to assess the relationships between saturated hydraulic conductivity and critical pore diameter. A strong correlation was found (r_s=0.97). This confirms the

importance of the critical pore diameter in the soil and its influence on hydraulic conductivity (Ghanbarian, Torres-Verdín, & Skaggs, 2016).

4. Summary and Conclusions

In this study, I used X-ray CT to investigate the volume of entrapped air in soil for defining its influence on measurements of saturated hydraulic conductivity in the laboratory. The method of upward saturation under a vacuum was applied in order to identify differences in the entrapped air content and its influence on measured K_s values. The study results have shown that the volume of entrapped air greatly depends on how the soil saturation was conducted. Moreover, the study found out that the constant-head laboratory method of K_s measurement at the SLU laboratory contributes to an extra penetration of air within the soil (mostly at the top and bottom parts of the cores). The saturated hydraulic conductivity and the entrapped air content were negatively correlated. Therefore, not considering the existence of the entrapped air leads to errors in estimating K_s values.

One limitation of the study is the amount of used samples. Only five samples were used for the analysis, which is not enough to make general inferences on the impact of air bubbles on soil Ks measurements.

Acknowledgments

References

Allison, L. (1947). Effect of Microorganisms on Permeability of Soil Under Prolonged Submergence. *Soil Science*, *63*(6), 439–450.

Bormann, H., & Klaassen, K. (2008). Seasonal and land use dependent variability of soil hydraulic and soil hydrological properties of two Northern German soils. *Geoderma*, *145*(3–4), 295–302. http://doi.org/10.1016/j.geoderma.2008.03.017

Christiansen, J. E. (1944). EFFECT OF ENTRAPPED AIR UPON THE PERMEABILITY OF SOILS. *Soil Science*, *58*(5), 355???366. http://doi.org/10.1097/00010694-194411000-00002

Dohnal, M., Jelinkova, V., Snehota, M., Dusek, J., & Brezina, J. (2013). Tree-dimensional numerical analysis of water flow affected by entrapped air: Application of noninvasive imaging techniques. *Vadose Zone Journal*, *12*(1). http://doi.org/10.2136/vzj2012.0078

Doube, M., Kłosowski, M. M., Arganda-Carreras, I., Cordelières, F. P., Dougherty, R. P., Jackson, J. S., … Shefelbine, S. J. (2010). BoneJ: Free and extensible bone image analysis in ImageJ. *Bone*, *47*(6), 1076–1079. http://doi.org/10.1016/j.bone.2010.08.023

Faybishenko, B. A. (1995). Hydraulic behavior of quasi-saturated soils in the presence of entrapped air: Laboratory experiments. *Water Resources Research*, *31*(10), 2421–2435. http://doi.org/10.1029/95WR01654

Feldkamp, I. A., Davis, L. C., & Kress, J. W. (1984). PRACTICAL CONE-BEAM ALGORITHM. *Journal of the Optical Society of America A: Optics and Image Science, and Vision*, *1*(6), 612–619.

Fodor, N., Sándor, R., Orfanus, T., Lichner, L., & Rajkai, K. (2011). Evaluation method dependency of measured saturated hydraulic conductivity. *Geoderma*, *165*(1), 60–68. http://doi.org/10.1016/j.geoderma.2011.07.004

GeoDict. (n.d.). Retrieved June 3, 2016, from http://www.geodict.com/

Ghanbarian, B., Torres-Verdín, C., & Skaggs, T. H. (2016). Quantifying tight-gas sandstone permeability via critical path analysis. *Advances in Water Resources*, *92*, 316–322. http://doi.org/10.1016/j.advwatres.2016.04.015

Helliwell, J. R., Sturrock, C. J., Grayling, K. M., Tracy, S. R., Flavel, R. J., Young, I. M., … Mooney, S. J. (2013). Applications of X-ray computed tomography for examining biophysical interactions and structural development in soil systems: a review. *European Journal of Soil Science*, *64*(3), 279.

Jelinkova, V., Snehota, M., Pohlmeier, A., van Dusschoten, D., & Cislerova, M. (2011). Effects of entrapped residual air bubbles on tracer transport in heterogeneous soil: Magnetic resonance imaging study. *Organic Geochemistry*, *42*(8), 991–998. http://doi.org/10.1016/j.orggeochem.2011.03.020

Katuwal, S., Norgaard, T., Moldrup, P., Lamandé, M., Wildenschild, D., & de Jonge, L. W. (2015). Linking air and water transport in intact soils to macropore characteristics inferred from X-ray computed tomography. *Geoderma*, *237–238*, 9–20. http://doi.org/10.1016/j.geoderma.2014.08.006

Klute, A., Campbell, G. S., & Soil Science Society of America. (1994). *Methods of soil analysis. P. 1, Physical and mineralogical methods*. Madison, Wis: SSSA.

Koestel, J., & Larsbo, M. (2014). Imaging and quantification of preferential solute transport in soil macropores. *Water Resources Research*, *50*(5), 4357–4378. http://doi.org/10.1002/2014WR015351

Larsbo, M., Koestel, J., & Jarvis, N. (2014). Controls of macropore network characteristics on preferential solute transport. *Hydrology and Earth System Sciences Discussions*, *11*, 9551–9588. http://doi.org/10.5194/hessd-11-9551-2014

Larsbo, M., Koestel, J., & Jarvis, N. (2014). Relations between macropore network characteristics and the degree of preferential solute transport. *Hydrology And Earth System Sciences*, *18*, 5255–5269. http://doi.org/10.5194/hess-18-5255-2014

Luo, L., Lin, H., & Li, S. (2010). Quantification of 3-D soil macropore networks in different soil types and land uses using computed tomography. *Journal of Hydrology*, *393*(1), 53–64. http://doi.org/10.1016/j.jhydrol.2010.03.031

Orlob, G. T., & Radhakrishna, G. N. (1958). The effects of entrapped gases on the hydraulic characteristics of porous media. *Transactions, American Geophysical Union*, *39*(4), 648. http://doi.org/10.1029/TR039i004p00648

Paradelo, M., Katuwal, S., Moldrup, P., Norgaard, T., Herath, L., & de Jonge, L. W. (2016). X-ray CT-Derived Soil Characteristics Explain Varying Air, Water, and Solute Transport Properties across a Loamy Field. *Vadose Zone Journal*, *15*(4), 0. http://doi.org/10.2136/vzj2015.07.0104

Preibisch, S., Saalfeld, S., Schindelin, J., & Tomancak, P. (2010). Software for bead-based registration of selective plane illumination microscopy data. *Nature Methods*, *7*(6), 418–419. http://doi.org/10.1038/nmeth0610-418

Sakaguchi, A., Nishimura, T., & Kato, M. (2005). effect of entrapped air on the quasi-saturated soil hydraulic conductivity and comparison with the unsaturated hydraulic conductivity. *Vadose Zone Journal VZJ*, *4*(1). Retrieved from http://vzj.scijournals.org/cgi/reprint/4/1/139

Schindelin, J., Arganda-Carreras, I., Frise, E., Kaynig, V., Longair, M., Pietzsch, T., … Cardona, A. (2012). Fiji: an open-source platform for biological-image analysis. *Nature Methods*, *9*(7), 676–682. http://doi.org/10.1038/nmeth.2019

Schneider, C. A., Rasband, W. S., & Eliceiri, K. W. (2012). NIH Image to ImageJ: 25 years of image analysis. *Nature Methods*, *9*(7), 671–675. http://doi.org/10.1038/nmeth.2089

Smith, R. M., & Browning, D. R. (1946). INFLUENCE OF EVACUATION UPON LABORATORY PERCOLATION RATES AND WETTING OF UNDISTURBED SOIL SAMPLES. *Soil Science*, *62*(3), 243–254. http://doi.org/10.1097/00010694-194609000-00004

Snehota, M., Jelinkova, V., Sobotkova, M., Sacha, J., Vontobel, P., & Hovind, J. (2015). Water and entrapped air redistribution in heterogeneous sand sample: Quantitative neutron imaging of the process. *Water Resources Research*, *51*(2), 1359–1371. http://doi.org/10.1002/2014WR015432

Stumm W, & Morgan J. J. (1996). Aquatic chemistry: chemical equilibria and rates in natural waters. 3rd ed.

Wildenschild, D., & Sheppard, A. P. (2013). X-ray imaging and analysis techniques for quantifying pore-scale structure and processes in subsurface porous medium systems. *Adv. Water Resour.*, *51*(1). http://doi.org/10.1016/j.advwatres.2012.07.018

Wildenschild, D., Vaz, C. M. P., Rivers, M. L., Rikard, D., & Christensen, B. S. B. (2002a). Using X-ray computed tomography in hydrology: systems, resolutions, and limitations. *Journal of Hydrology*, *267*(3–4), 285–297. http://doi.org/10.1016/S0022-1694(02)00157-9

Wildenschild, D., Vaz, C. M. P., Rivers, M. L., Rikard, D., & Christensen, B. S. B. (2002b). Using X-ray computed tomography in hydrology: systems, resolutions, and limitations. *Journal of Hydrology*, *267*(3), 285–297. http://doi.org/10.1016/S0022-1694(02)00157-9